Prepared for submission to JINST

15TH Topical Seminar on Innovative Particle and Radiation Detectors
14-17 October 2019
Siena, Italy

# Micrometric laser characterization of a 300 μm fully-depleted monolithic active pixel sensor in standard 110 nm CMOS technology

**R. A. Giampaolo[a,b] on behalf of the ARCADIA collaboration**

[a] *Department of Electronics and Telecommunications, Politecnico di Torino, Corso Duca degli Abruzzi 24, 10129 Torino*
[b] *INFN Torino, Via Pietro Giuria 1, 10125 Torino, Italy*

*E-mail:* raffaele.giampaolo@polito.it

Abstract: This work presents the characterization of a customized 110 nm CMOS technology fully depleted monolithic active pixel sensor test structure through micrometric laser beam. The test structures, with removed electronics, enabled transient current technique evaluation of the collected charge with two laser wavelengths. High charge collection uniformity and full depletion are proved using front-side illumination in the sensitive areas.

Keywords: Particle tracking detectors; Photon detectors for UV, visible and IR photons (solidstate); Photon detectors for UV, visible and IR photons (solid-state) (PIN diodes, APDs, Si-PMTs, G-APDs, CCDs, EBCCDs, EMCCDs, CMOS imagers, etc)

## Contents



## 1 Introduction

Research and development on fully depleted monolithic active pixel sensors (FD-MAPS) are driven by the growing interest in the high energy physics, medical and space application communities in fully depleted sensors with charge collection dynamics dominated by drift [1, 2]. Two common approaches are HV-CMOS and SOI-based technologies. In HV-CMOS, the very front-end electronics is embedded in the collection electrodes leading to fairly high input capacitance, which implies higher power consumption for a given space resolution [3]. The SOI sensor requires, on the other hand, a highly customized process to properly handle and overcome back-gate effects, the coupling between the high voltage bias and the front end electronics and to improve radiation hardness [4].

This work presents the characterization of the sensitive area of a customized $110\,\mathrm{nm}$ CMOS FD-MAPS. Full depletion implies higher bulk radiation tolerance. The adoption of an n type substrate enables the usage of deep p-wells and small n collection electrodes increasing the signal to noise ratio. The main sensor characteristics are discussed in section 2 while a description of the used test structure is in section 3. The first TCT (Transient Current Technique) scans performed on the test structures, demonstrating the functionality of the device and full depletion, are in section 4.

## 2 Sensor characteristics

The produced FD-MAPS, shown in Figure 1, implements the electronics in a deep p-well embedded in an n-doped epitaxial layer. The deep p-well effectively decouples the n-doped high resistivity substrate from the electronics [6]. The highly doped epitaxial layer reduces the resistivity and facilitates the control of the electrostatic potential below the deep p-wells.

The sensitive diode of the device is located in the backside and consists in a p+/nsub junction. The p+ implantation is made after thinning the substrate and is activated with laser annealing. The adoption of an n-type substrate, in conjunction with a back p+ implantation, enables the application of high potentials to the back side rather than near the collecting electrodes. Furthermore, guard rings along the p+ perimeter allow to sustain the high voltage needed to uniformly deplete the full

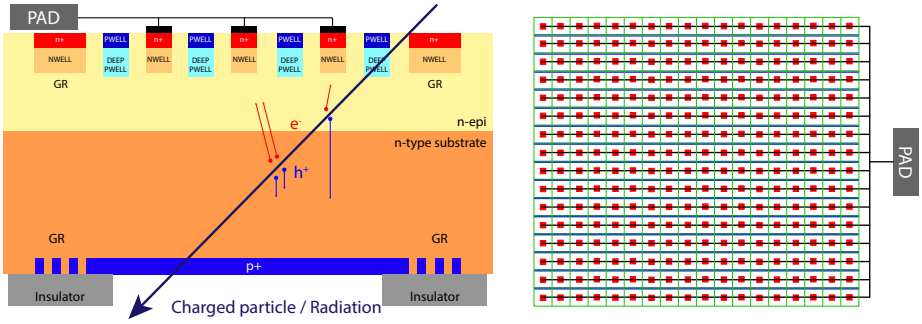


**Figure 1**. *Left*: Section (not to scale) of a test structure *right*: top view of the matrix (*green*), full metal stack (*blue*) and metal lines (*black*) connecting all the pixel electrodes (*red*).

sensor thickness. This peculiar design implies that the depletion starts from the backside and moves upwards through the substrate. Thus, a signal from an interacting particle or photon can only be acquired once the depletion layer has reached the top collecting electrodes.

Despite the backside implants, the sensor fabrication is fully compatible with a standard CMOS production line and does not require an ad-hoc solution for the processing of the front side.

## 3 Test structure

The test structure consists of a matrix of $16 \times 18$ square pixels, each with a pitch of $25\,\mu\mathrm{m}$. All the pixels are connected in parallel so that the signals can be readout by means of one pad, as depicted in Figure 1. The test structure used in this work has been designed to test the sensor properties independently from the implemented electronic circuits and for this reason, it does not contain transistors within the p-well.

A 6-layer aluminium stack, with an $8\,\mu\mathrm{m}$ width and a $2.32\,\mu\mathrm{m}$ total thickness, has been included, in blue in Figure 1. The stack metal lines are parallel to the lines for signal collection and are located on the edge of each pixel to minimize the metal coverage. The stack can also be used to study the front side illumination worst case in which most photons are reflected and particles would lose part of their energy.

A top guard ring (GR) has been designed, via an n-well implantation, on the perimeter of the matrix array to isolate the pixels from the parasitic edge currents.

The GR, p-wells and electrode pads have been connected, via wire bonding, to a small carrier PCB to bias the structures externally, while the p+ bottom electrode has been connected to the PCB metal area via conductive adhesive in order to bias it uniformly. The direct connection to the electrodes enables substrate characterization via standardized sensor test setups.

## 4 Experimental results

The charge collection investigation has been performed at the Ruđer Bošković Institute in Zagreb using a TCT scan equipment by Particulars [7, 8]. This standard technique adopts a pulsed laser beam to evaluate the performance of solid state particle detectors. The beam produces free carrier pairs which are then collected by the electrodes.

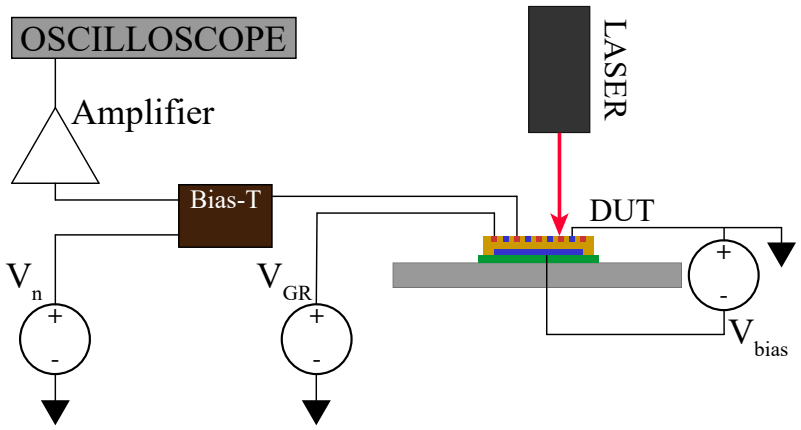


**Figure 2**. Illustration of the experimental setup. The p-wells of test structure have been connected to the common ground and its back side has been connected to the bias voltage, $V_{bias}$.

Two picosecond laser wavelengths were chosen for the characterization, namely $\lambda_{red} = 660\,\mathrm{nm}$ and $\lambda_{IR} = 1064\,\mathrm{nm}$. The first wavelength, $\lambda_{red}$, is absorbed within the first 3 to 5 µm yielding information on the structure and charge collection profiles of the surface. The second wavelength is absorbed in about 800 µm of silicon implying that, for a 300 µm sample, the ionization trail is similar to the one of a minimum ionizing particle (MIP).

The test setup is sketched in Figure 2. A Particulars BT-01 Bias-T has been connected to the output pad of the electrodes to impose the bias voltage and decouple it from the high frequency signal to be acquired. In series with the BT-01, a wide-band Particulars amplifier with a 53 dB gain has been connected. The sample is then fixed onto a micrometrically controlled stage perpendicular to the laser beam.

Table 1 reports the bias voltages, needed to operate the sensor in full depletion, applied to the GR, n electrodes, p-wells and on the p+ bottom electrode. The voltages are as follows:

**Table 1**. Bias Voltages

| $V_{GR}$ | $V_n$ | $V_{p-well}$ | $V_{bias}$ |
|---|---|---|---|
| 1.2 V | 1.2 V | 0 V | −150 V |

The data acquisition was done with a Lecroy waverunner WR8404M-MS oscilloscope at 20 GS/s rate. To remove noise, the signal averaging was set to 50 samples. A 2D map of the pixel array surface is obtained combining the signal from the acquisition chain to the beam location. Steps of 2 µm were taken in the x and y direction and the acquired signals are integrated. The step size was set smaller than the beam spot, which was focused evaluating the minimum signal in z-y scans near the matrix edges, where the z axis is the beam direction. The beam spot diameter was estimated to be smaller than the pixel active area, but larger than the metalizations. Nonetheless, the characterization of collection uniformity and full depletion are still possible adopting a spot size smaller than the pixel sensitive area.

The first test, aimed to characterize the sensor surface, adopted the $\lambda_{red} = 660\,\mathrm{nm}$ monochromatic source with a peak power of 10 mW.

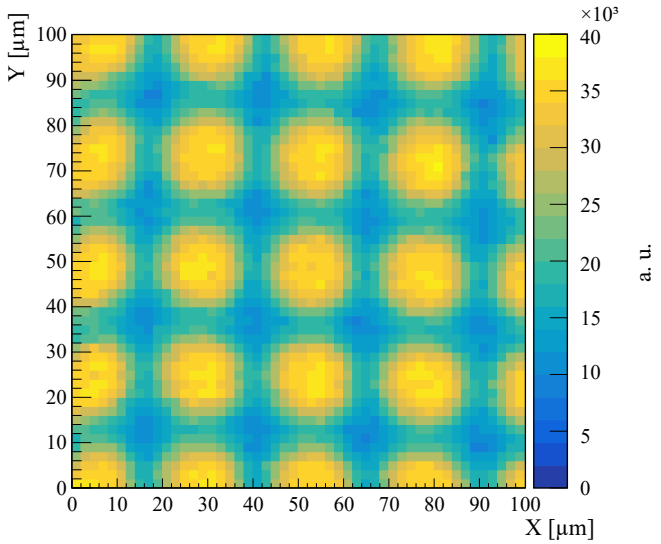


**Figure 3**. TCT integral scan of the previously studied 100 µm × 100 µm sensor area using the $\lambda_{red}$ = 660 nm laser source.

After validating the functionality of the whole sensor, a 2D map of the central $100 \times 100\,\mu\mathrm{m}^2$ zoomed area is acquired and shown in Figure 3. The laser was collimated via a cut of the beam width of 60 % and the frequency was set to 50 Hz. The colormap is proportional to the acquired signal integrated in a time window, $T_{int}$ = 8 ns, which includes the full signal. The n-well sensitive volume can be seen as the uniform high integrated charge structures. The low integral structures identify the p-wells. The latter structures are, in fact, not sensitive to incoming photons and the $\lambda_{Red}$ penetration depth is comparable to the p-well thickness, decreasing the effective signal amplitude.

The second test adopted an IR wavelength illumination. The laser beam, with a peak power of 100 mW, was collimated by 40 % to emulate hundreds of MIP crossings. At a $\lambda_{IR}$ = 1064 nm, full thickness crossing is expected and, in turn, a high number of carriers. The same area as the previous test has been analyzed and the 2D map acquired of the integrated signal, with the same integration time $T_{int}$, is visible in Figure 4.

The results illustrate the blockage effect of the 6-metal stack and inter-metal dielectric. The inferred metal width is compatible with the designed layout of 8 µm. Via vertical cuts along the n-wells and metal lines, in Figure 4, a low standard deviation over value ratio, s = 3.9%, is measured which implies a high charge collection uniformity.

In order to evaluate the number of MIPs acquired, two waveforms, one over the collection electrodes and one over the metal lines, have been chosen for numerical integration:

$$\begin{cases} I_{IR,n-well} = 14.45 \text{ nWb} \\ I_{IR,metal} = 8.47 \text{ nWb} \end{cases} \tag{4.1}$$

This calculation implies, for a 300 µm thick silicon sensor, an estimated number of ≈ 170 MIP crossings. The decrease in charge collection is expected over metal lines due to laser reflections and its spot size larger than the metal lines. Evaluating the ratio of the two integrated signals, an effective beam spot diameter $d < 20$ µm can be found. This value does not take into account the beam profile, but confirms the initial estimation.

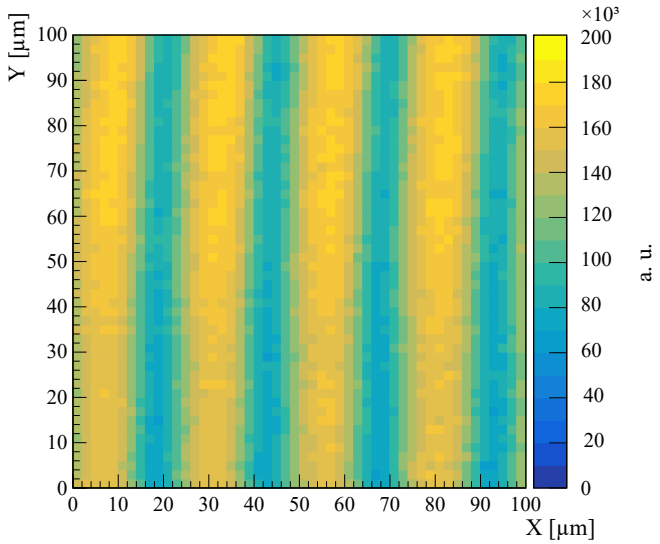


**Figure 4**. TCT scan of a $100\,\mu\mathrm{m} \times 100\,\mu\mathrm{m}$ sensor area using the $\lambda_{IR} = 1064\,\mathrm{nm}$ laser source.

Comparing the IR and the red source results, full sensor depletion is proved considering: the high sensitivity below the p-wells, the equivalent charge collection efficiency below the n-wells and p-wells when switching to the IR laser source and, finally, the 8 ns time required for complete charge collection, which implies drift-dominated collection dynamics.

## 5 Conclusions

A test structure of the monolithic active pixel sensor, deprived of the electronics blocks, has been produced for a detailed characterization of the substrate material and collecting electrodes. Full depletion to 300 µm has been proved, implying the possibility of adopting the sensor for radiation tracking purposes. Via TCT scans, the charge collection has been demonstrated to be uniform in the active regions using both IR and red laser beams. Further proof of uniformity has been achieved via microbeam proton tests, [9], and neutron irradiation campaigns to characterize radiation hardness are ongoing.

## Acknowledgments

This project has received funding from the European Union's Horizon 2020 Research and Innovation programme under Grant Agreement no. 654168, 669014.

We thank our colleagues at the RBI in Zagreb for their help carrying out our tests in their facilities and in the results analyses: M. Bezak, V. Chmill, M. Kalliokoski and A. Karadzhinova-Ferrer. Furthermore, we thank F. Dumitrache, B. Pini and M. Tornago from INFN Torino.

## References

[1] W. Snoeys, J. D. Plummer, S. Parker and C. Kenney, *PIN detector arrays and integrated readout circuitry on high-resistivity float-zone silicon*, *IEEE Trans. Electron Devices*, **1** (1994) 903

[2] W. Snoeys et al., *A process modification for CMOS monolithic active pixel sensors for enhanced depletion, timing performance and radiation tolerance*, *Nucl. Instr. Meth. A*, **871** (2017) 90-96

[3] I. Peric, *A novel monolithic pixelated particle detector implemented in high-voltage CMOS technology*, *Nucl. Instr. Meth. A*, **582** (2007) 876

[4] W. Kucewicz et al., *Fully depleted monolithic active pixel sensor in SOI technology*, *IEEE Nucl. Sci. Symp. Conf. Rec.*, **2** (2004) 1227

[5] S. Lauxtermann et al., *A monolithic 640 × 512 CMOS imager with high-NIR sensitivity*, *Infrared Technology and Applications XL*, **9070** (2014) 907002

[6] L. Pancheri et al., *A 110nm CMOS process for fully-depleted pixel sensors*, 2019 *JINST*, **14** C06016

[7] G. Kramberger, *Advanced Transient Current Technique Systems*, *The 23rd International Workshop on Vertex Detectors* (2014) 032

[8] J. Bronuzzi et al., *Principle and modelling of Transient Current Technique for interface traps characterization in monolithic pixel detectors obtained by CMOS-compatible wafer bonding*, 2016 *JINST*, **11** P08016

[9] L. Pancheri et al., *Fully depleted MAPS in 110nm CMOS process with 100 - 300* µm *active substrate*, *IEEE Trans. Electron Devices*, **67** (2020) 2393